Comput Mech (2007) 40:901–909
DOI 10.1007/s00466-006-0149-3

ORIGINAL PAPER

An implicit BEM formulation to model strong discontinuities in solids

O. L. Manzoli · W. S. Venturini

Received: 3 February 2006 / Accepted: 16 November 2006 / Published online: 21 December 2006

Abstract A boundary element method (BEM) formulation to predict the behavior of solids exhibiting displacement (strong) discontinuity is presented. In this formulation, the effects of the displacement jump of a discontinuity interface embedded in an internal cell are reproduced by an equivalent strain field over the cell. To compute the stresses, this equivalent strain field is assumed as the inelastic part of the total strain. As a consequence, the non-linear BEM integral equations that result from the proposed approach are similar to those of the implicit BEM based on initial strains. Since discontinuity interfaces can be introduced inside the cell independently on the cell boundaries, the proposed BEM formulation, combined with a tracking scheme to trace the discontinuity path during the analysis, allows for arbitrary discontinuity propagation using a fixed mesh. A simple technique to track the crack path is outlined. This technique is based on the construction of a polygonal line formed by segments inside the cells, in which the assumed failure criterion is reached. Two experimental concrete fracture tests were analyzed to assess the performance of the proposed formulation.

Keywords Boundary elements · Fracture mechanics · Cohesive models · Strong discontinuity

O. L. Manzoli (✉)
Department of Civil Engineering, São Paulo State University,
Av. Luiz Edmundo C. Coube, S/N,
17033-360 Bauru, SP, Brazil
e-mail: omanzoli@feb.unesp.br

W. S. Venturini
São Carlos School of Engineering, University of São Paulo,
Av. Trabalhador São-carlense, 400,
13566-590 São Carlos, SP, Brazil
e-mail: venturin@sc.usp.br

1 Introduction

In the last two decades, a considerable efforts have been made to predict structural failure in computational solid mechanics. Initiation and growth of displacement discontinuities (strong discontinuities), such as cracks in quasi-brittle materials or slip lines in metals or granular materials, must be properly modeled to achieve the critical load as well as to describe the post-critical behavior.

The main difficulties arise from the multiscale character of problems involving occurrence of discontinuities. Standard continuum theory is not able to properly describe the very localized material degradation that precedes the formation of strong discontinuities. The use of strain-softening constitutive relations to model the degradation of the mechanical properties induces material instability with strain localization in thin bands. In the absence of some physical limitation, the most stable state is achieved when the width of the localization band vanishes.

In the context of the finite element method (FEM) the width of the band is limited to the domain of a single continuous element, which causes the known spurious mesh-size and mesh-bias dependence. Many enhanced continuum theory such as non-local, gradient-enhanced, micropolar and viscous-regularized continuum have been proposed to overcome this pathological mesh dependence by introducing an intrinsic length as the minimum localization bandwidth. By doing this, the finite element discretization no longer defines the size of the expected localization region. It should be just fine enough to properly describe the high strain gradient in the localization region. This ensures convergence of the results with mesh refinement.

On the other hand, in the context of concrete fracture mechanics, displacement discontinuity is assumed since the first stage of material failure when the fictitious crack model proposed by Hillerborg [9] is adopted. The material degradation process (fracture process), that precedes the crack definition, is described by a discrete (cohesive) constitutive relationship between traction and displacement discontinuity along the crack surface. Standard continuum theory is kept to describe the continuum portion of the solid.

In the continuum strong discontinuity approach first introduced by Simo et al. [27] (see also references [23,20, 19,17]), it has been demonstrated that the standard continuum (stress-strain) constitutive model can be applied even for unbounded strains that are compatible with discontinuous displacement fields. It also has been proved that the continuum constitutive model projects onto the discontinuity interface in the form of a discrete (traction-displacement) constitutive model. In this context, Oliver [18] and Oliver et al. [20] have proposed an efficient approach based on the regularized version of the strong discontinuity formulation, in which stresses along the interface are obtained by using the strains computed from a regularized discontinuity displacement field over a very small (finite) width.

From the numerical point of view, the distinction between modeling the continuum and the crack interface is source of difficulties. The introduction of new boundaries or interface elements to model the crack propagation, whose location is unknown prior to the analysis, requires a sophisticate mesh regeneration technique [3].

To avoid using mesh regeneration to find the crack path, solid finite elements with embedded displacement discontinuities (also referred to as embedded crack elements), have been proposed by many authors [11]. Since discrete cracks can be introduced into these finite elements during the analysis without regard to the mesh topology, arbitrary crack path propagation can be efficiently modeled using a fixed mesh, provided that a suitable technique for tracking the crack is used.

In the context of the boundary element methods, the dual version first developed by Portela et al. [24] for elastic fracture mechanics and later extended to deal with fictitious crack models with an arbitrary crack path by Saleh and Aliabadi [2,25] has proved to be a very efficient technique. It is important to mention that the cohesive crack model has also been used together with BEM formulations, as can be seen in Liang and Li [12] and Cen and Maier [7], who have used this model together with the classical sub-region technique, in Lopes Jr. and Venturini [13] and Jiang and Venturini [10], in which dipole corrections were used to model 2D and 3D cohesive crack problems, and in Chen et al. [8] where the well known symmetric Galerkin BEM approach was adopted. A comprehensive review of the use of the boundary element methods in fracture mechanics can be found in [1].

In this paper, the same principle behind the finite element with embedded discontinuity, proposed by Oliver [18] and Oliver et al. [20], is applied to simulate discontinuity propagation using boundary element method. Following the concepts shown by Manzoli and Shing [14], instead of trying to represent the discontinuity itself, the proposed approach introduces the effect of the discontinuity in a small region adjacent to the discontinuity line. This neighbor region consists of internal cells containing the discontinuity line that propagates during the analysis. The effect of the embedded discontinuity is taken into account by properly approaching the strain field over the cell domain, reproducing the equivalent strain relaxation of the continuum portion of the cell due to the discontinuity. Thus, the discontinuity effects are smeared out across the internal cell in a consistent way. By taking this aspect into account, one can solve problems involving discontinuities in the implicit boundary element method framework [5,4].

2 Internal cell with embedded discontinuity

Let us consider an internal triangular cell whose domain Ω_c with an inside discontinuity interface S_c splitting the cell into two sub-domains, leaving one corner (the solitary corner) separate from the other two, as shown in Fig. 1. Let us denote $\mathbf{n}_c$ and $\mathbf{m}_c$ the unit vectors normal to S_c and to the cell boundary opposite the solitary corner, respectively. The vector $[\![\mathbf{u}]\!]$ standing for the displacement jump on S_c, contains the components of the relative displacement between the opposite sides of S_c. If the displacement jump is uniform along S_c, the relative rigid-body motion between the two parts of the cell corresponds to a relative translation.

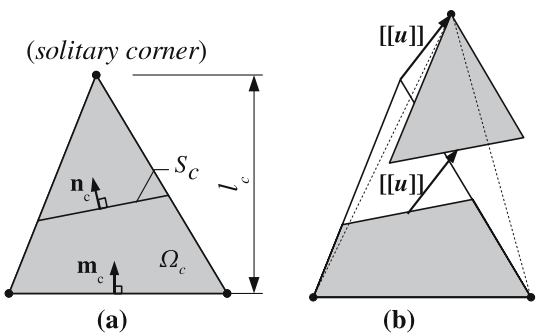

Fig. 1 Internal cell with embedded discontinuity

The relative displacements between the cell corners produced by the rigid-body translation (see Fig. 1) can also be related to a uniform strain field over the entire cell, whose expression is given by:

$$\bar{\boldsymbol{\epsilon}} = \frac{1}{l_c}\,(\mathbf{m}_c \otimes [\![\mathbf{u}]\!])^S \tag{1}$$

where $(\bullet)^S$ is the symmetric part of $(\bullet)$, $\otimes$ denotes the tensorial product and l_c is the characteristic length of the cell, defined as the distance between the solitary corner and its opposite cell boundary (see Fig. 1). Then, $\bar{\boldsymbol{\epsilon}}$ can be regarded as the equivalent strain field that results from smearing the displacement jump, $[\![\mathbf{u}]\!]$, over the entire cell domain in a consistent way, according to Eq. (1).

The strain field over the cell, $\boldsymbol{\epsilon}$, can be decomposed into two parts: the first one related to the deformation of the continuum portion of the cell and denoted by $\tilde{\boldsymbol{\epsilon}}$, and the second part related to the displacement jump of the discontinuity interface, $\bar{\boldsymbol{\epsilon}}$:

$$\boldsymbol{\epsilon} = \tilde{\boldsymbol{\epsilon}} + \bar{\boldsymbol{\epsilon}} \tag{2}$$

For the sake of simplicity, the material of the solid portion is assumed linearly elastic. In this case, the stress field over the cell is given by

$$\boldsymbol{\sigma} = \mathbf{C} : (\boldsymbol{\epsilon} - \bar{\boldsymbol{\epsilon}}) \tag{3}$$

in which $\mathbf{C}$ is the elastic fourth order constitutive tensor defined by $\mathbf{C} = [2G\nu/(1-2\nu)]\mathbf{1}\otimes\mathbf{1} + 2G\mathbf{I}$, where $\mathbf{1}$ and $\mathbf{I}$ are the second and fourth order unit tensors, respectively, ν is the Poisson's ratio and G is the shear modulus. A more general formulation, with dissipative effects in the bulk, could be considered by replacing relation (3) by a nonlinear constitutive relation based on plasticity or damage theory, for instance.

2.1 Nonlinear behavior of the interface

The traction vector in the discontinuity interface can be related to the jumps by means of a discrete (cohesive) constitutive law of the form:

$$\mathbf{t}_S = \boldsymbol{\Sigma}^d([\![\mathbf{u}]\!]) \tag{4}$$

where $\boldsymbol{\Sigma}$ denotes the discrete (traction-displacement jump) constitutive law, which gives the traction vector along the interface for a given displacement jump and its history.

Alternatively, one can write the interface discontinuity displacement as the limit situation of a strain localization band whose width tends to zero [21] by following the regularized strong discontinuity approach [18]. In this case the traction vector can be related to the strain along the interface by means of a continuum (stress–strain) constitutive relation. Thus, the traction vector reads

$$\mathbf{t}_S = \mathbf{n}_c \cdot \boldsymbol{\Sigma}^c(\boldsymbol{\epsilon}_S) \tag{5}$$

where $\boldsymbol{\epsilon}_S$ gives the interface strain and $\boldsymbol{\Sigma}^c$ denotes the continuum constitutive law.

The strain in the interface can be approximated by [16]

$$\boldsymbol{\epsilon}_S = \tilde{\boldsymbol{\epsilon}} + \frac{1}{k}(\mathbf{n}_c \otimes [\![\mathbf{u}]\!])^S \tag{6}$$

or

$$\boldsymbol{\epsilon}_S = \boldsymbol{\epsilon} - \frac{1}{l_c}\,(\mathbf{m}_c \otimes [\![\mathbf{u}]\!])^S + \frac{1}{k}(\mathbf{n}_c \otimes [\![\mathbf{u}]\!])^S \tag{7}$$

Parameter k in Eqs. (6) and (7) can be regarded as the width of the very narrow band containing S_c, across which the displacement discontinuity is regularized. Then, the last component of the strain field presented in Eqs. (6) and (7) corresponds to the strains that result from the regularization of the displacement discontinuity. When k tends to zero the discrete approach is recovered and the continuum constitutive law is transformed into a discrete one, provided that some requirements are fulfilled by the continuum constitutive law [17,21].

2.2 Traction continuity condition

The tractions evaluated over the continuum portion and along the interface inside the cell must be equal to enable the continuum and interface coupling. This continuity condition reads:

$$\mathbf{t}_S - \mathbf{n}_c \cdot \boldsymbol{\sigma} = \mathbf{0} \tag{8}$$

By substituting Eqs. (4) and (3) into Eq. (8) and taking into account the relations (1), the traction continuity condition for the discrete approach can be expressed as

$$\boldsymbol{\Sigma}^d([\![\mathbf{u}]\!]) - \mathbf{n}_c \cdot \mathbf{C} : \left(\boldsymbol{\epsilon} - \frac{1}{l_c}\,(\mathbf{m}_c \otimes [\![\mathbf{u}]\!])^S\right) = \mathbf{0} \tag{9}$$

On the other hand, by replacing Eqs. (5) and (7) into (8) one obtains the traction continuity for the regularized strong discontinuity approach, given by the following form:

$$\mathbf{n}_c \cdot \boldsymbol{\Sigma}^c\left(\boldsymbol{\epsilon} - \frac{1}{l_c}\,(\mathbf{m}_c \otimes [\![\mathbf{u}]\!])^S + \frac{1}{k}(\mathbf{n}_c \otimes [\![\mathbf{u}]\!])^S\right) - \mathbf{n}_c \cdot \mathbf{C} : \left(\boldsymbol{\epsilon} - \frac{1}{l_c}\,(\mathbf{m}_c \otimes [\![\mathbf{u}]\!])^S\right) = \mathbf{0} \tag{10}$$

2.3 Equivalent continuum constitutive relation

In order to compute the stresses from the total strain over the cell, one has to identify the part of the total

strain resulting from the continuous portion deformation. From a given total strain field at a cell internal point, the displacement jump $[\![\mathbf{u}]\!]$ can be found locally by solving the nonlinear system of equations defined by imposing the traction continuity condition, Eq. (9) (or (10)), using the strain tensor, $\boldsymbol{\epsilon}$, evaluated at the chosen point. Since the exact position of the discontinuity inside the cell is irrelevant, the collocation point can always be placed at the center.

Once the jump is found, the strains corresponding to the discontinuity interface can be obtained from Eq. (1). Then, the stresses can be evaluated by the linearly elastic relation given by Eq. (3).

This procedure used to obtain the stresses in the continuum portion from a given total strain field in the interior of the cell with the presence of a discontinuity interface can be interpreted as an equivalent continuum constitutive relation, which is herein denoted by $\hat{\boldsymbol{\Sigma}}$. Thus, the stresses in the continuum region can be written in terms of the current total strains as follows:

$$\boldsymbol{\sigma} = \hat{\boldsymbol{\Sigma}}(\boldsymbol{\epsilon}) \tag{11}$$

According to the procedure outlined previously, the stresses over the cell are also given in terms of the total strain and its history (reflected by the internal variables of the interface constitutive model), the cell geometry and the discontinuity interface position inside the cell ($\mathbf{m}_c$, $\mathbf{n}_c$ and l_c).

Note that the resulting formulation tries to reproduce the correct kinematic effect of the discontinuity in the cell and, at the same time, enforces the equilibrium condition at the interface. In the context of the FEM, these ingredients generate the so-called statically and kinematically optimal non-symmetric formulation (SKON), that renders non-symmetric stiffness matrix. Alternative formulations leading to symmetric finite element equations can be achieved by relaxing the kinematic or the static condition (see reference [11] for more details). In the context of the BEM, the non-symmetry of the resulting equations is not influenced by these conditions.

3 Implicit BEM equations

Let us consider an elastic solid Ω with boundary Γ, containing an inelastic narrow region Ω^i over which an inelastic field of strains $\boldsymbol{\epsilon}^i$ is applied. The usual displacement boundary integral equations for a collocation point ζ, in absence of body forces, is given by [6]:

$$\mathbf{c}_\zeta \cdot \mathbf{u} = \int_\Gamma \mathbf{p}\cdot\mathbf{u}^*\mathrm{d}\Gamma - \int_\Gamma \mathbf{u}\cdot\mathbf{p}^*\mathrm{d}\Gamma + \int_{\Omega^i} \boldsymbol{\epsilon}^i : \boldsymbol{\sigma}^*\mathrm{d}\Omega \tag{12}$$

where $\mathbf{u}$ and $\mathbf{p}$ are boundary displacement and traction vectors, respectively, and $\mathbf{p}^*$, $\mathbf{u}^*$ and $\boldsymbol{\sigma}^*$ are the known Kelvin's elastic fundamental solutions. The $\mathbf{c}_\zeta$ matrix depends on the position of the collocation point ζ.

Replacing the inelastic strain by the total and elastic strain parts, $\boldsymbol{\epsilon}^i = \boldsymbol{\epsilon} - \mathbf{C}^{-1} : \boldsymbol{\sigma}$, one obtains:

$$\mathbf{c}_\zeta \cdot \mathbf{u} = \int_\Gamma \mathbf{p}\cdot\mathbf{u}^*\mathrm{d}\Gamma - \int_\Gamma \mathbf{u}\cdot\mathbf{p}^*\mathrm{d}\Gamma + \int_{\Omega^i} (\boldsymbol{\epsilon} - \mathbf{C}^{-1} : \boldsymbol{\sigma}) : \boldsymbol{\sigma}^*\mathrm{d}\Omega \tag{13}$$

The integral expression of the strains compatible with the displacement field of Eq. (13) at internal collocation points is given as [6]

$$\boldsymbol{\epsilon} = \int_\Gamma \mathbf{p}\cdot\mathbf{U}^*\mathrm{d}\Gamma - \int_\Gamma \mathbf{u}\cdot\mathbf{P}^*\mathrm{d}\Gamma + \int_\Omega \mathbf{b}\cdot\mathbf{U}^*\mathrm{d}\Gamma + \int_{\Omega^i} (\boldsymbol{\epsilon} - \mathbf{C}^{-1} : \boldsymbol{\sigma}) : \boldsymbol{\Sigma}^*\mathrm{d}\Omega + (\boldsymbol{\epsilon} - \mathbf{C}^{-1} : \boldsymbol{\sigma}) : \boldsymbol{\Xi}^* \tag{14}$$

where $\mathbf{U}^*$, $\mathbf{P}^*$, and $\boldsymbol{\Sigma}^*$ are the symmetric gradient of Kelvin's elastic fundamental solutions, taken with respect to the coordinates of the collocation point.

The last term in Eq. (14) arising from the derivative of the singular integral of the inelastic term of Eq. (13) reads:

$$\boldsymbol{\Xi}^* = -\frac{1}{8(1-\nu)}\left[2(3-4\nu)\,\mathbf{I} - (1-4\nu)\,\mathbf{1}\otimes\mathbf{1}\right] \tag{15}$$

As usual for BEM formulations the non-linear problem represented by Eqs. (13) and (14) can be solved by transforming them into algebraic representations. This is obtained by dividing the boundary Γ into n_e boundary elements, Γ_e (e = 1, 2 , ..., n_e), and the sub-region Ω^i of the domain into n_c internal cells, Ω_c (c = 1, 2, ..., n_c), over which the geometry and the variables of the problem can be approximated in terms of nodal values. After performing the relevant integrals over boundary elements and internal cells, one can write the discretized form of the displacement equation for each boundary node to obtain the following set of algebraic equations:

$$[\mathbf{H}]\{\mathbf{u}\} = [\mathbf{G}]\{\mathbf{p}\} + [\mathbf{Q}]\left(\{\boldsymbol{\epsilon}\} - \{\mathbf{C}^{-1} : \boldsymbol{\sigma}\}\right) \tag{16}$$

where $\{\mathbf{u}\}$ and $\{\mathbf{p}\}$ are vectors collecting the nodal boundary values and, $\{\boldsymbol{\epsilon}^{\boldsymbol{i}}\}$, $\{\boldsymbol{\epsilon}\}$ and $\{\boldsymbol{\sigma}\}$ are the vectors representing the inelastic strains, the total strains and the stresses in the internal cells, respectively.

By grouping the unknown nodal variables into a vector $\{\mathbf{y}\}$, Eqs. (16) can be rewritten as

$$[\mathbf{A}]\{\mathbf{y}\} = \{\mathbf{f}\} + [\mathbf{Q}]\left(\{\boldsymbol{\epsilon}\} - \{\mathbf{C}^{-1} : \boldsymbol{\sigma}\}\right) \tag{17}$$

where $\{\mathbf{f}\}$ is the vector of forces corresponding to the prescribed nodal displacements and tractions.

In the same way, another set of equations can be obtained by writing the discretized form of the strain integral equation (14) for collocation points in the internal cells, rendering

$$\{\boldsymbol{\epsilon}\} = [\mathbf{A}']\{\mathbf{y}\} + \{\mathbf{f}'\} + [\mathbf{Q}']\left(\{\boldsymbol{\epsilon}\} - \{\mathbf{C}^{-1} : \boldsymbol{\sigma}\}\right) \tag{18}$$

By substituting vector $\{\mathbf{y}\}$ obtained from Eq. (17) into Eq. (18) and taking into account that the stress in each cell can be obtained from the total strain according to the relation (11), Eq. (18) becomes the following system of nonlinear equations in terms of the total strains:

$$\{\boldsymbol{\epsilon}\} = \{\mathbf{m}\} + [\mathbf{S}]\left(\{\boldsymbol{\epsilon}\} - \{\mathbf{C}^{-1} : \hat{\boldsymbol{\Sigma}}(\boldsymbol{\epsilon})\}\right) \tag{19}$$

with

$$\{\mathbf{m}\} = \{\mathbf{f}'\} - [\mathbf{A}'][\mathbf{A}]^{-1}\{\mathbf{f}\} \tag{20}$$

$$[\mathbf{S}] = [\mathbf{Q}'] - [\mathbf{A}'][\mathbf{A}]^{-1}[\mathbf{Q}] \tag{21}$$

where $\{\mathbf{m}\}$ is the purely elastic solution.

The nonlinear system of equation (19) can then be implicitly solved for the strains by means of an iterative technique combined with an incremental procedure. The incremental procedure is obtained by multiplying the force vectors $\mathbf{f}$ and $\mathbf{f}'$ in the previous equations by the loading factor λ_n, which scales the loading level for the nth loading increment. By doing this, the incremental form of the system of equations (19) can be written as:

$$\{\boldsymbol{\epsilon}_n\} - \lambda_n\{\mathbf{m}\} - [\mathbf{S}]\left(\{\boldsymbol{\epsilon}_n\} - \{\mathbf{C}^{-1} : \hat{\boldsymbol{\Sigma}}(\boldsymbol{\epsilon}_n)\}\right) = \mathbf{0} \tag{22}$$

which can be solved for the strains corresponding to the nth loading increment, $\boldsymbol{\epsilon}_n$, by means of the iterative Newton–Raphson method. Once the strains are found, the corresponding boundary unknowns can be obtained from Eq. (17) and the loading factor can be updated for the next increment.

4 Concrete fracture analysis

Modeling concrete fracture problems requires an interface constitutive model to describe the main features of the concrete failure under tension, as well as a scheme for tracking the crack path during the analysis. In this paper, these specific ingredients are chosen as follows:

4.1 Interface constitutive law

The nonlinear behavior in the interface is provided by the regularized strong discontinuity approach outlined in Sect. 2.1. The material along the interface line is described by the standard associative elastoplastic constitutive model, which can be described by the following set of rate equations [26]:

$$\dot{\boldsymbol{\sigma}} = \mathbf{C}\,(\dot{\boldsymbol{\epsilon}} - \dot{\boldsymbol{\epsilon}}^p) \tag{23}$$

$$\dot{\boldsymbol{\epsilon}}^p = \dot{\lambda}\,\frac{\partial \phi}{\partial \boldsymbol{\sigma}} \tag{24}$$

$$\dot{\alpha} = \dot{\lambda} \tag{25}$$

$$\dot{q} = H(\alpha)\,\dot{\alpha} \tag{26}$$

where $\mathbf{C}$ is the elastic material matrix, $\dot{\boldsymbol{\epsilon}}^p$ is the plastic strain vector, $\dot{\lambda}$ is the plastic multiplier, α is the strain-like internal variable, q is the softening internal variable, and H is the softening modulus.

The loading and unloading situations are distinguished by the Kuhn–Tucker conditions:

$$\phi(\boldsymbol{\sigma}, q) \le 0, \quad \dot{\lambda} \ge 0, \quad \dot{\lambda}\,\phi(\boldsymbol{\sigma}, q) = 0 \tag{27}$$

where ϕ is the yield function which defines the elastic domain when $\phi(\boldsymbol{\sigma}, q) < 0$.

To describe the mixed-mode crack behavior in quasi-brittle materials, the following expressions for the yield surface and softening law are adopted:

$$\phi(\boldsymbol{\sigma}, q) = \sqrt{\frac{2}{3}}\,\|\mathbf{S}\| + p - q \tag{28}$$

$$q = f_t\, e^{-\frac{f_t}{G_F}k\alpha}; \quad H = \frac{\partial q}{\partial \alpha} = -k\frac{f_t^2}{G_F}e^{-\frac{f_t}{G_F}k\alpha} \tag{29}$$

where $p = Tr(\boldsymbol{\sigma})/3$ is the mean stress, $\mathbf{S} = \boldsymbol{\sigma} - p\mathbf{I}$ stands for the deviatoric stresses, f_t is the tensile strength, G_F is the fracture energy and k is the regularization strong discontinuity parameter defined in Sect. 2.1.

The exponential evolution law of the stress-like variable q, given by Eq. (29), ensures dissipation compatible with the fracture energy, G_F, which is considered as a material property (see reference [21]).

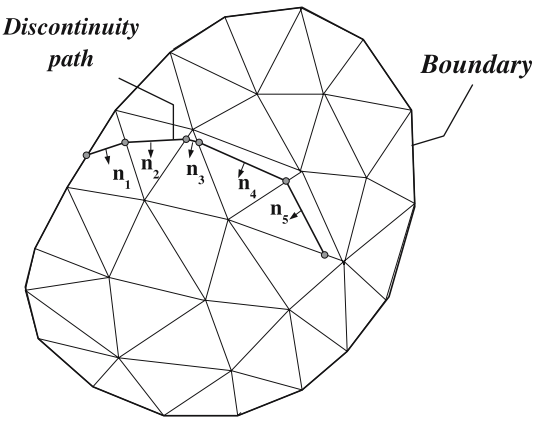

Fig. 2 Tracking scheme to trace the discontinuity path

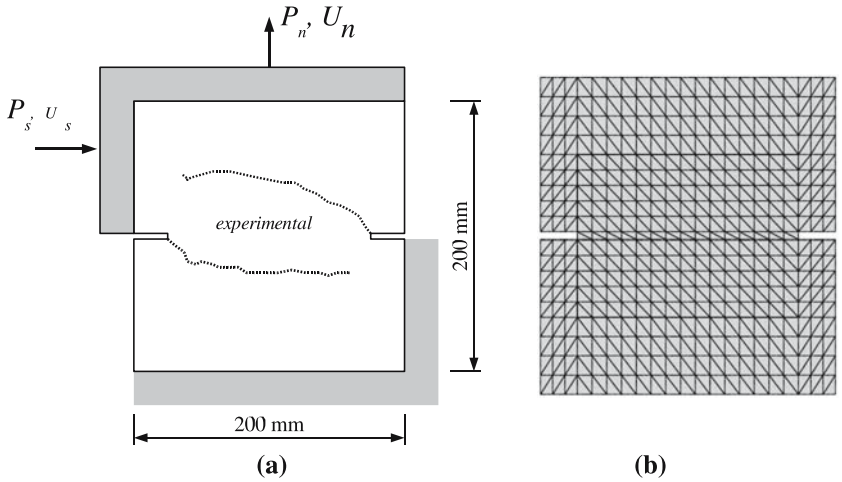

Fig. 3 Nooru test: **a** geometry and boundary conditions; **b** internal cell discretization

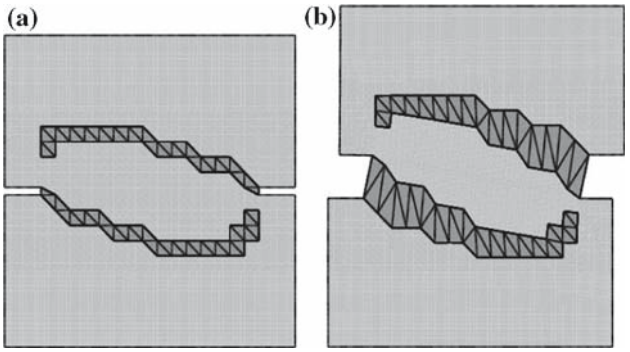

Fig. 4 Numerical results at the end of the analysis: **a** internal cells containing the crack path; **b** deformed mesh

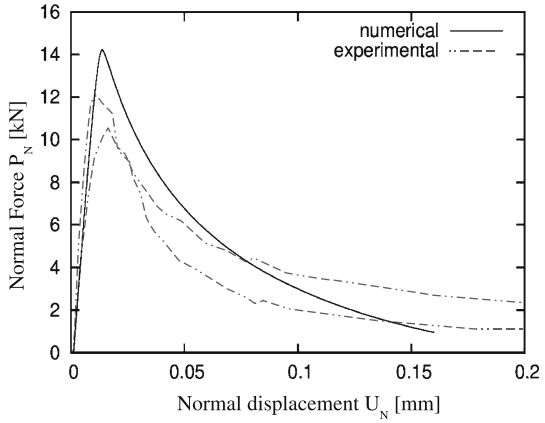

Fig. 5 Nooru test. Normal (vertical) force, P_N, versus normal (vertical) displacement of the top edge, U_N

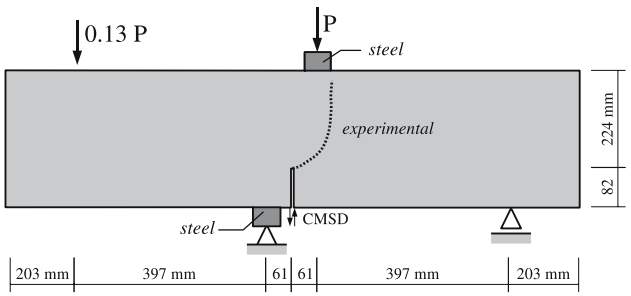

Fig. 6 Four-point bending test. Geometry and boundary conditions

4.2 Tracking the crack path

Since the position and direction of crack propagation in general are not known prior to an analysis, an algorithm is developed to track the crack that propagates during the loading. A polygonal line is constructed by sequentially adding straight crack segments in the internal cells whose stress state reaches the failure criterion. The process starts from the first cell that reaches the failure criterion and propagates through its neighbor cells, keeping continuity of the crack across the cell boundaries (see Fig. 2). Only the cell that has one side "touching" the crack tip is allowed to fail causing crack propagation. In this approach the computation of the direction of a crack and the checking of the failure criterion are based on the stress state at the center of the cell. The crack initiation criterion coincides with the plastic yield criterion of the interface constitutive law and the direction of the propagation is taken as the maximum principal stress direction at the crack initiation time.

The procedure outlined here is able to track one crack line propagating from the first element that reaches the failure criterion. Propagation of few crack lines can also be modeled if the first cell of each potential crack line is identified prior to the analysis. This simple technique is suitable for the numerical studies performed in this paper. A more general technique for tracking multiple cracks is provided in reference [22].

Only those cells containing the crack path are required to be computed in the nonlinear system of equation (19), which becomes larger as the crack

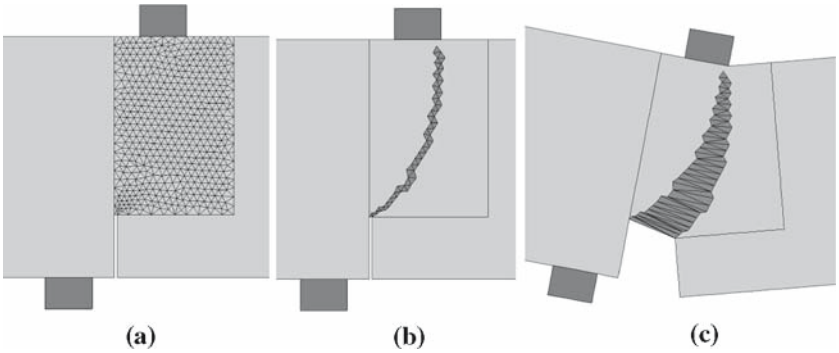

Fig. 7 Four-point bending test. **a** Internal cells; **b** internal cells containing the crack path; **c** deformed mesh

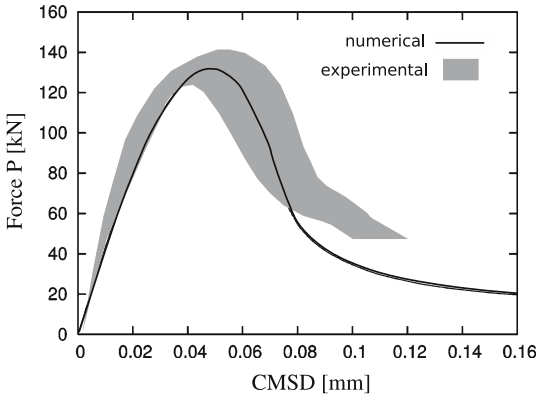

Fig. 8 Four-point bending test. Force versus CMSD curves

propagates. This feature drastically reduces the computation effort to solve the nonlinear problem.

4.3 Concrete fracture tests

4.3.1 Double-edge-notched specimen

To assess the performance of the model to simulate propagation of curved crack paths, the double-edge notched plain concrete specimen tested by Nooru-Mohamed [15] was chosen for the numerical study. Simulations in the context of the finite element method can be found in reference [28]. In this test, a concrete square with deep notches on both sides was subjected first to a shear (horizontal) load $P_S = 10\,\text{kN}$ and then to a normal (vertical) tensile load P_N under displacement control, while keeping the shear load constant. The geometry and boundary conditions of the test are depicted in Fig. 3a. The numerical simulation was performed by distributing the shear force on the upper left edge and imposing an increasing vertical displacement along the top edge, so that the normal load was computed as the resulting reaction force. The assumed material properties are: Young's modulus $E = 32\,\text{GPa}$, Poisson's ratio $\nu = 0.18$, yield stress $\sigma_y = 3.75\,\text{MPa}$ and fracture energy $G_F = 100\,\text{N/m}$. The regularization parameter was $k = 1\,\text{mm}$ and plane stress was assumed with an out-of-plane thickness of 50 mm.

To impose this non-proportional loading, the forces vectors $\mathbf{f}$ and $\mathbf{f}'$ were replaced by $\mathbf{f}_S + \lambda_n \mathbf{f}_N$ and $\mathbf{f}'_S + \lambda_n \mathbf{f}'_N$, respectively, in the boundary element equations of Sect. 3. λ_n is the loading factor corresponding to the nth loading increment, $\mathbf{f}_S$ and $\mathbf{f}'_S$ are the force vectors due to the shear load and $\mathbf{f}_N$ and $\mathbf{f}'_N$ are the ones corresponding to the prescribed vertical displacement on the top edge.

Figure 3b shows the mesh used in the boundary element discretization of the specimen. Cracks are allowed to propagate from the two cells located near the notch tips. Although the entire domain is divided into internal cells, only those cells that were crossed by the crack path during the loading process took part in the nonlinear analysis.

Figure 4a shows only the internal cells containing the crack lines at the end of the analysis. As can be observed, the crack pattern predicted by the numerical model is very close to that of the experimental test. The deformed specimen (enlarged 150 times) at the end of the analysis is shown in Fig. 4b. As expected, it can be seen that the high deformation of the cells reproduces the crack discontinuity modes. Figure 5 shows the normal load-displacement curve of the numerical model and the experimental tests. Despite some scatter, the numerical model is able to represent well the behavior observed during the test.

4.3.2 Four-point bending test

The notched concrete beam test, which geometry and boundary conditions are shown in Fig. 6, is also analyzed. The results of this experimental test have been reported by Arrea and Ingraffea [3]. The assumed parameters are: Young's modulus $E = 32\,\text{GPa}$, Poisson's ratio $\nu = 0.18$, yield stress $\sigma_y = 2.5\,\text{MPa}$, fracture energy $G_F = 100\,\text{N/m}$ and regularization parameter $k = 1\,\text{mm}$. Plane stress was assumed with out-of-plane thickness of 155 mm.

Figure 7a shows the unstructured internal cell mesh used in the region where the crack was expected to form. One crack line was allowed to initiate from the internal cell located near the notch tip. The set of internal cells crossed by the crack line at the end of the analysis is shown in Fig. 7b, giving a good prediction of the crack position observed in the experiment. As can be seen in Fig. 7c, the localized deformation in those cells reflects the crack discontinuity modes. Figure 8 shows the evolution of the load, P, with respect to the crack mouth sliding displacement, CMSD. The numerical analysis was able to give a good prediction of the structural behavior of the specimen, even with the very simple interface constitutive model adopted.

5 Conclusions

A BEM formulation has been proposed to simulate strong discontinuity in solid mechanics. The formulation is based on internal cells with embedded discontinuities. The kinematics of the discontinuity is taken into account by introducing an equivalent inelastic strain field over the cell, which is designed to be a consistent distribution of the displacement jump across the cell interior. The nonlinear behavior associated to the discontinuity interfaces can be described by a discrete (traction-displacement) constitutive relation, as in the fictitious crack model, or by means of a continuum (stress–strain) constitutive model in the context of the strong discontinuity approach. By enforcing traction continuity between discontinuity interface and continuum at collocation points over the internal cells, it is possible to obtain the stresses in the continuum portion of the cells from the total strains. This allows for the problem involving discontinuity to be solved in the implicit BEM framework.

The formulation showed suitable for fracture mechanics analyzes with arbitrary crack paths. Only boundary variables and the equivalent inelastic strain in the interior cells containing the discontinuity are approximated.

The main purpose of this work has been to introduce the concepts of the strong discontinuity approach, originally developed in the context of the FEM, in the BEM. A comparative study of the performance of both methods will be addressed in future work.

Acknowledgments The authors wish to acknowledge the financial support from the State of São Paulo Research Foundation (FAPESP).

References

1. Aliabadi MH (1997) Boundary element formulations in fracture mechanics. Appl Mech Rev 50:83–96
2. Aliabadi MH, Saleh AL (2002) Fracture mechanics analysis of cracking in plain and reinforced concrete using the boundary element method. Eng Fract Mech 69:267–280
3. Arrea M, Ingraffea AR (1982) Mixed-mode crack propagation in mortar and concrete. Dept Struct Eng Rep 81–13
4. Benallal A, Fudoli CA, Venturini WS (2002) An implicit bem formulation for gradient plasticity and localization phenomena. Int J Numer Method 53:1853–1869
5. Bonnet M, Mukherjee S (1996) Implicit bem formulations for usual and sensitivity problems in elasto-plasticity using the consistent tangent operator concept. Int J Solids Struct 33(30):4461–4480
6. Brebbia CA, Telles JCF, Wrobel LC (1984) Boundary element techniques. Springer, Berlin Heidelberg New York
7. Cen Z, Maier G (1992) Bifurcations and instabilities in fracture of cohesive-softening structures: a boundary element analysis. Fatigue Fract Eng Mater 15:911–928
8. Chen T, Wang B, Cen Z, Wu Z (2002) A symmetric galerkin multi-zone boundary element method for cohesive crack growth. Eng Fract Mech 63:591–609
9. Hillerborg A, Modeer M, Petersson PE (1976) Analysis of crack formation and crack growth in concrete by means of fracture mechanics and finite elements. Cement Concrete Res 6:773–782
10. Jiang YS, Venturini WS (2000) A general boundary element method for analysis of slope stability. In: Roeck G, Topping BHV (eds) Computational civil and structural engineering. Civil-comp Press, pp 191–198
11. Jirásek M (2000) Comparative study on finite elements with embedded discontinuities. Comp Methods Appl Mech Eng 188:307–330
12. Liang RY, Li YN (1992) Simulations of non-linear fracture process zone in cementitious material a boundary element approach. J Comput Mech 7(4):413–427
13. Lopes MC Jr., Venturini WS (1997) Cohesive crack analysis by the boundary element method. In: Owen DRJ, Onate E, Hinton E (eds) Proc. international conference on computational plasticity V. Barcelona, CIMNE, pp 1057–1062
14. Manzoli OL, Shing PB (2006) A general technique to embed non-uniform discontinuities into standard solid finite elements. Comput Struct 84:742–757
15. Nooru-Mohamed MB (1992) Mixed-mode fracture of Concrete: an experimental approach. PhD thesis, Delft University of Technology
16. Oliver J (1995) Continuum modelling of strong discontinuities in solid mechanics using damage models. Comput Mech 17(1–2):49–61
17. Oliver J (1996) Modeling strong discontinuities in solid mechanics via strain softening constitutive equations. part 1: Fundamentals. Int J Num Meth Eng 39(21):3575–3600
18. Oliver J (1996) Modeling strong discontinuities in solid mechanics via strain softening constitutive equations. part 2: Numerical simulation. Int J Num Meth Eng 39(21):3601–3623
19. Oliver J (2000) On the discrete constitutive models induced by strong discontinuity kinematics and continuum constitutive equations. Int J Solids Struct 37:7207–7229
20. Oliver J, Cervera M, Manzoli OL (1997) On the use of j2 plasticity models for the simulation of 2d strong discontinuities in solids. In: Owen DRJ, Onate E, Hinton E (eds) Proc. international conference on computational plasticity V. Barcelona, CIMNE, pp 38–55

21. Oliver J, Cervera M, Manzoli OL (1999) Strong discontinuities and continuum plasticity models: the strong discontinuity approach. Int J Plasticity 15(3):319–351
22. Oliver J, Huespe AE, Samaniego E, Chaves EWV (2004) Continuum approach to the numerical simulation of material failure in concrete. Int J Numer Anal Methods Geomech 28:609–632
23. Oliver J, Simó JC (1994) Modelling strong discontinuities by means of strain softening contitutive equations. In Mang H et al. (eds) Proc. EURO-C 1994 computer modelling of concrete structures Swansea. Pineridge Press, pp 363–372
24. Portela A, Aliabadi MH, Rooke DP (1992) Dual boundary element method: efficient implementation for cracked problems. Int J Numer Methods Eng 33:1269–1287
25. Saleh AL, Aliabadi MH (1995) Crack growth analysis using boundary element method. Eng Fract Mech 51:533–545
26. Simó JC, Hughes TJR (1998) Computational Inelasticity. Springer, Berlin Heidelberg New York
27. Simó JC, Oliver J, Armero F (1993) An analysis of strong discontinuities induced by strain-softening in rate-independent inelastic solids. Comput Mech 12:277–296
28. Spencer B (2002) Finite elements with embedded discontinuities for modeling reinforced concrete members, PhD thesis, University of Colorado